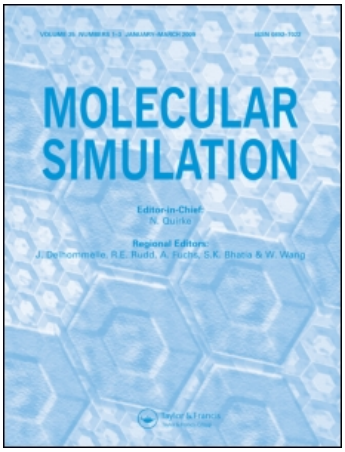


**Molecular Simulation**
Publication details, including instructions for authors and subscription information:
http://www.informaworld.com/smpp/title~content=t713644482

# Dynamic properties of methane, water and methane hydrates using computational simulations

F. Castillo-Borja[a]; R. Vázquez-Román[b]; U. I. Bravo-Sánchez[a]
[a] Departamento de Ingeniería Química, Instituto Tecnológico de Aguascalientes, Aguascalientes, Ags, Mexico [b] Departamento de Ingeniería Química, Instituto Tecnológico de Celaya, Celaya, Gto, Mexico

First published on: 02 September 2009

**To cite this Article** Castillo-Borja, F. , Vázquez-Román, R. and Bravo-Sánchez, U. I.(2010) 'Dynamic properties of methane, water and methane hydrates using computational simulations', Molecular Simulation, 36: 3, 229 — 239, First published on: 02 September 2009 (iFirst)
**To link to this Article: DOI:** 10.1080/08927020903196930
**URL:** http://dx.doi.org/10.1080/08927020903196930

*Molecular Simulation*
Vol. 36, No. 3, March 2010, 229–239

Taylor & Francis
Taylor & Francis Group

# Dynamic properties of methane, water and methane hydrates using computational simulations

F. Castillo-Borja[a]*, R. Vázquez-Román[b] and U.I. Bravo-Sánchez[a]

[a]*Departamento de Ingeniería Química, Instituto Tecnológico de Aguascalientes, Av. López Mateos 1801 Ote, Fracc. Bona Gens, Aguascalientes, Ags., CP 20256, Mexico;* [b]*Departamento de Ingeniería Química, Instituto Tecnológico de Celaya, Av. Tecnológico s/n, Celaya, Gto., CP 38010, Mexico*

(*Received 20 March 2009; final version received 20 July 2009*)

In this study, the vibrational spectrum of methane hydrates is calculated through dynamic molecular simulations based on two different methods. The spectra obtained using the proposed procedure allow the differentiation of the contributions of different inter- and intramolecular motion types in the spectrum, which cannot be produced with the traditional method based on atomic velocities. Simulations were carried out at different composition, pressure and temperature conditions to observe the effect of these variables on the vibrational spectrum. The proposed method allowed the observation of a difference in the frequencies for the C—H stretching vibrations between small and large cavities, which agrees with reported experimental values.

**Keywords:** methane hydrate; molecular dynamics; vibrational spectrum; autocorrelation functions



## 1. Introduction

Hydrates are solids consisting of water molecules, which form a crystal lattice where certain molecules, referred as guest, remain trapped. The guest molecules can behave as either gas or liquid while remaining outside the hydrate, but the molecular size must be small enough so as to fit into the cavities and big enough to be retained inside the cavities. Compounds known to form hydrates include methane, carbon dioxide, propane and isobutane, among others. In particular, the analysis of methane hydrates has received greater attention lately since the natural existence of a great quantity of them has been proved to exist and they can offer a possible energy source in the future. The most typical crystalline form of methane hydrates is structure I (sI) [1], in which the cubic unit cell contains 46 water molecules which arrange themselves in different ways around methane molecules distributed in two small and six large cavities.

Several experimental techniques have been explored to determine the structures and compositions of hydrates as well as to increase the knowledge of their thermodynamic properties and formation kinetics. It includes crystallographic analysis of X-ray diffraction [2,3], NMR [4], Raman [5–9] and IINS studies [10]. Raman spectroscopy seems to be the preferred technique since a great number of studies have recently been reported it as a technique simpler than the NMR, not destructive and with the advantage of being easy to carry out *in situ* even at extreme conditions of temperature and pressure. Also, the study of methane hydrates using Raman spectroscopy is the method of choice because the scattering cross section of water is very low and thus permits the observation of the whole Raman spectrum of the guest, while in the IR spectrum, only small windows are left by the strong water absorptions and, in neutron scattering, the hydrogen from water could hardly be separated from the hydrogen of methane.

Most spectroscopic investigations of methane hydrates have been focused on the analysis of the stretching vibrations of the methane molecule in the small and large cavities of the hydrate. In particular, the symmetric C—H vibration provides excellent means to discriminate hydrate cavities, but it is not good to identify the type of the hydrate because the difference in the frequency for this vibration for similar cavities between structures I and II is about $2\,cm^{-1}$. Sum et al. [5] have used Raman spectroscopy to evaluate the frequencies of methane in different cavities of hydrates sI. The splitting of the band for methane in the hydrate corresponds to the occupation of the two different types of cavities. The band for the small cavity appears at $2915\,cm^{-1}$ and the band for the large cavity occurs at $2904.8\,cm^{-1}$. The two frequencies correspond to the symmetric C—H stretching mode in methane. The intensity of the band for methane in the large cavity is greater than that for the small cavity in the hydrate sI since the ratio of large to small cavities is 3:1. These results seem to indicate that almost all the large cavities in the methane hydrate sI are occupied whereas just a small fraction of the small cavities remain occupied. There is an increase in the occupation of both cavities when the temperature and the pressure increase, implying that methane will remain trapped in the hydrate.

Simulation techniques such as molecular dynamics (MD) are very useful to find the relationship among the

*Corresponding author. Email: floriannecb@gmail.com

ISSN 0892-7022 print/ISSN 1029-0435 online

DOI: 10.1080/08927020903196930
http://www.informaworld.com

bands from the experimental spectroscopic analysis and the appropriate time correlation functions from the data collected in the MD simulations. The methodology of the MD has been extensively used to study a great variety of thermodynamic, structural and dynamic properties of hydrates. This technique allows atomic-level modelling based on the knowledge of interatomic forces and assumptions from classical mechanics. MD is often used to imitate the reality, to develop experiments which are not feasible and to calculate functions which are not directly measurable. Thus, dynamic properties from MD can be related to experimental results. For instance, the vibrational spectrum or vibrational density of states simulated in MD can be related to experimental results of incoherent inelastic neutron scattering (IINS) and spectroscopic methods such as Raman and IR.

The vibrational spectrum of methane hydrates has been evaluated through MD simulations, producing good agreement with some experimental data of IR [11,12]. However, the spectrum associated with the molecular motion in these works reflects only the translation contributions because methane is described as a single site of interaction. In addition, MD simulations with rigid models can only provide direct information of the low-frequency region corresponding to the translational motions of the molecules. MD calculations of intramolecular motions at higher frequencies have been usually based on the Fourier transform of the atomic velocity autocorrelation function (VACF) using flexible force fields. Several MD works report the methane hydrates' vibrational spectrum obtained from the VACF using flexible models for the molecular description [13–16]. However, in these computer simulations, the vibrational spectrum of methane hydrates has been calculated for a single thermodynamic condition, and, hence, it is not possible to analyse the effect of the thermodynamic conditions in the bands of the vibrational spectrum. The spectra calculated by Itoh and Kawamura [13] were carried out at 1 atm and 100 K for liquid methane and at 100 atm and 100 K for methane hydrate; the NVT simulation of Greathouse and Cygan [15] was performed at 273 K for methane hydrate and methane gas; English and MacElroy [14] and Jiang et al. [16] performed a NPT simulation at 200 K and 20 bar for methane hydrate. In most of the above-mentioned studies, the numerical vibrational spectrum of methane hydrate was compared with experimental results, although the Raman spectra were collected near 273 K [5].

The first objective of the present study is to analyse the vibrational spectra of the guest molecules in methane hydrate at different pressures and temperatures. In addition, the vibrational spectra of water- and methane-free molecules were calculated to determine the change in the vibrational frequency of the molecules when incorporated into the hydrate.

The bands of the vibrational spectrum related to the different types of motions can be unequivocally identified by choosing as a spectroscopy property a coordinate such as atomic displacements or velocities or combinations, associated with a given motion. Martí et al. [17] have analysed several procedures with MD simulations to calculate the IR spectrum for liquid water at room temperature. One of these procedures allows the differentiation of the contributions of different inter- and intramolecular motion types in the spectrum, which cannot be produced with the traditional method based on atomic velocities. For this reason, our second objective of this study is to apply this simple method which approximates the essential features of the normal coordinate motions to compare eventually the calculated spectra with those produced with the method based on atomic velocities.

## 2. Computational details

Methane hydrates are explicitly simulated by considering the atoms of oxygen, carbon and hydrogen. Several flexible models of force fields for water and methane have been reported. The TJE model [18] is used in this study to describe the potential of water molecules and the OPLS-AA model [19] for methane molecules. Both the TJE and OPLS-AA models appropriately predict the properties of pure substances in wide ranges of temperature and pressure. The analytic form of the force field $u(r_{ij})$ for both the models includes interactions of non-bonding and allows internal changes in the molecular structure. The flexibility is imposed by using harmonic terms for the stretching and bending of the angles. The above-mentioned interactions are given by

$$u(r_{ij}) = \sum_i \sum_{j>i} \left( 4\varepsilon_{ij} \left[ \left( \frac{\sigma_{ij}}{r_{ij}} \right)^{12} - \left( \frac{\sigma_{ij}}{r_{ij}} \right)^{6} \right] + \frac{1}{4\pi\varepsilon_0} \frac{q_i q_j}{r_{ij}} \left[ 1 + \frac{\varepsilon_{RF} - 1}{2\varepsilon_{RF} + 1} \left( \frac{r_{ij}}{r_c} \right)^3 \right] \right) + \sum_{\text{all bonds}} \frac{1}{2} k_b (d_{ij} - r_0)^2 + \sum_{\text{all angles}} \frac{1}{2} k_\theta (\theta - \theta_0)^2, \quad (1)$$

where $r_{ij}$ is the distance between the atoms $i$ and $j$; $\sigma_{ij}$ and $\varepsilon_{ij}$ are the Lennard-Jones parameters; $q_i$ and $q_j$ are the electrostatic charges of the atoms; $r_c$ is the cut-off radius that is just half the box length; $\varepsilon_0$ is the permittivity of the empty space and $\varepsilon_{RF}$ is the dielectric constant of the reaction field method whose arbitrarily fixed value is $\varepsilon_{RF} = \infty$; $k_b$ is the force constant for bond stretching between the atoms $i$ and $j$; $d_{ij}$ and $r_0$ are the instantaneous and equilibrium bond lengths, respectively; $k_\theta$ is the force constant for the angle bending among covalent bonds of atoms $i$, $j$ and $k$; $\theta$ and $\theta_0$ are the instantaneous and equilibrium angles, respectively. The corresponding parameters are given in Table 1. The parameters of

Table 1. Parameters for water and methane.

| Water | | Methane | |
|---|---|---|---|
| Parameter | Value | Parameter | Value |
| $\theta_0$ H—O—H | 109.47° | $\theta_0$ H—C—H | 107.8° |
| $r_0$ O—H | 1 Å | $r_0$ C—H | 1.09 Å |
| $k_\theta$ H—O—H | 46,065 K/rad$^2$ | $k_\theta$ H—C—H | 33212.9 K/rad$^2$ |
| $k_b$ O—H | 557711.2 K/Å$^2$ | $k_b$ C—H | 342193.9 K/Å$^2$ |
| $\varepsilon_{OO}$ | 78.2 K | $\varepsilon_{CC}$ | 33.2 K |
| $\sigma_{OO}$ | 3.166 Å | $\sigma_{CC}$ | 3.5 Å |
| $q_O$ | −0.82 e | $\varepsilon_{HH}$ | 15.09 K |
| $q_H$ | 0.41 e | $\sigma_{HH}$ | 2.5 Å |
| | | $q_C$ | −0.24 e |
| | | $q_H$ | 0.06 e |

Table 1 are used with the Lorentz–Berthelot combination rules to determine the values of the Lennard-Jones parameters in the case of non-electrostatic interactions between water and methane molecules.

The simulation box consists of a cubic lattice where periodic boundary conditions are applied throughout the simulation to avoid surface effects. The integration of the equations of motion was made through the velocity Verlet algorithm [20]. The Berendsen thermostat and barostat [21] were used to keep both the temperature and the pressure constant. During the production time, the atomic velocities as well as other properties are stored to perform appropriate analysis. In this analysis, the autocorrelation functions of these properties are evaluated and later transformed to the frequency domain to build the vibrational spectrum. Finally, the main bands from the spectrum are assigned to specific inter- or intramolecular vibrations.

### 2.1 Method of atomic velocities

It should be emphasised that, due to the analysis method based on the Fourier transform of the VACF, the obtained vibrational spectrum lacks information on the dipole moment transitions and on the polarisability of the system. Therefore, the heights of the bands obtained in the numerical spectrum do not really reflect the absorption or the scattering intensity of an IR or a Raman spectrum, respectively. However, the frequencies of the bands obtained in the numerical spectrum are comparable to the bands' positions in the experimental Raman spectra.

In this method, the vibrational spectrum $f(\omega)$ of the atomic movements is obtained through the Fourier transform of the VACF:

$$f(\omega) = \int_0^\infty \exp(-i\omega t)\langle v(t)\cdot v(0)\rangle dt, \tag{2}$$

$$\langle v(t)\cdot v(0)\rangle = \frac{1}{N}\sum_{i=1}^{N}\langle v_i(t)\cdot v_i(0)\rangle, \tag{3}$$

where $v(t)$ and $v(0)$ are the velocity of an atom at time $t$ and starting time, respectively. The angular parentheses represent averages on the number of molecules and on several origins in time.

Each vibrational spectrum was obtained from the autocorrelation functions of the methane atomic velocities, which were averaged from stored velocities at every five integration steps during 500 integration steps. The resolution of the spectra obtained after applying the Fourier transform was 4 cm$^{-1}$.

### 2.2 Method of atomic velocity decomposition

This method is based on the original idea of Bopp [22] to analyse the normal modes of vibration in liquid water. The method is based on the decomposition of the instantaneous velocities of hydrogen atoms with respect to the molecular centre of mass in its parallel and perpendicular components to the molecular plane. The parallel component is also decomposed in its parallel ($B_i(t) = B_i e_i(t)$) and perpendicular ($A_i(t) = A_i g_i(t)$) components to the OH direction (Figure 1), where $i$ refers to the hydrogen in the water molecule.

The following spectroscopic properties resulting by combining velocity components are defined:

$$Q_1(t) = B_1(t) + B_2(t), \tag{4}$$

$$Q_3(t) = B_1(t) - B_2(t), \tag{5}$$

where $Q_1(t)$ and $Q_3(t)$ are combinations of the atomic movements along the OH direction, and they approximately describe the symmetric and asymmetric stretching vibrations, respectively. The previous method for water was adapted for the methane molecule. In the present study, each of the instantaneous velocities of the two hydrogen atoms of every triplet H—C—H of the methane molecule in the molecular centre-of-mass system is projected onto the instantaneous unit vectors in the directions of the corresponding C—H bond. The spectroscopic quantities $Q_1(t)$ and $Q_3(t)$ on the molecular plane are calculated, according to Equations (4) and (5), to represent

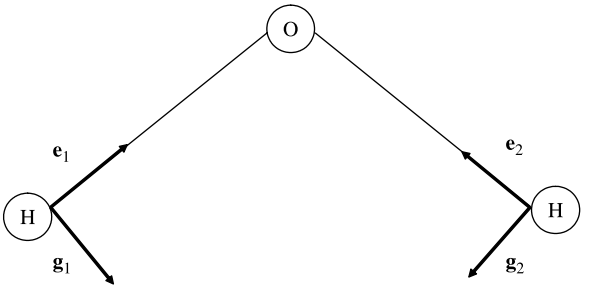


Figure 1. Vectors used in the velocity decomposition method for the water molecule.

the symmetric and asymmetric stretching vibrations, respectively. The most obvious way of assigning vibrations would be to use linear combinations of internal coordinates; however, the atomic positions in molecular mechanics are invariably expressed in terms of Cartesian coordinates, unlike quantum mechanics, where internal coordinates are often used.

The methane molecule has nine normal modes of vibration, from which the C—H symmetric stretching ($\sim 2900\,\mathrm{cm}^{-1}$), two bending vibrations ($\sim 1500$ and $\sim 1300\,\mathrm{cm}^{-1}$) and the asymmetric stretching vibration ($\sim 3000\,\mathrm{cm}^{-1}$) appear with high intensity in the Raman spectrum [23]. From these four vibrational modes, the first one has received greater attention in the Raman spectroscopic studies of methane hydrates since it appears with more intensity with respect to the other ones [24]. In this way, the method of atomic velocity decomposition will approximately allow the assignation of the bands in the vibrational spectrum to the normal modes of methane in the hydrate.

In this method of velocity decomposition, the vibrational spectrum $f(\omega)$ is obtained through the Fourier transform of the autocorrelation function for the spectroscopic property $A(t)$, which can represent any of the above described $Q_1(t)$ and $Q_3(t)$ properties, i.e.

$$f(\omega) = \int_0^\infty \exp(-\mathrm{i}\omega t)\langle A(t)\cdot A(0)\rangle \mathrm{d}t, \tag{6}$$

$$\langle A(t)\cdot A(0)\rangle = \frac{1}{N}\sum_{i=1}^{N}\langle A(t)\cdot A(0)\rangle, \tag{7}$$

where $A(t)$ and $A(0)$ are the spectroscopic properties for the molecule at time $t$ and starting time, respectively. The angular parentheses represent averages on the number of molecules and on several origins in time.

Each vibrational spectrum using the method of velocity decomposition was obtained from Equations (6) and (7) and the $Q_1(t)$ and $Q_3(t)$ properties were calculated at every five integration steps. The autocorrelation functions were calculated during 500 integration steps and then they were averaged. After applying the Fourier transform, the resolution of the obtained spectra was $4\,\mathrm{cm}^{-1}$.

## 3. Results

The structure of the hydrates depends not only on the guest molecule but also on the pressure and temperature conditions. The aim of the first three cases indicated in Table 2 was to compare the Raman spectroscopic studies with the vibrational frequencies obtained by NPT simulations in this work. The calculated vibrational frequencies for methane hydrate (case 1 of Table 2) were compared with experimental data [5]. Additionally, the spectra obtained for methane dissolved in water and for gaseous methane were compared with experimental information for the same conditions [7]. Several simulations indicated in Table 2 were carried out in this study where the pressure was fixed for various temperature values and vice versa. The purpose is to detect whether any of these changes can appear in the vibrational spectrum of the hydrate. Vibrational spectra for each of the analysed thermodynamic conditions were calculated using the two previously described methods.

Table 2. Analysed thermodynamic conditions.

| Case | System | Temperature (K) | Pressure (MPa) |
|---|---|---|---|
| 1 | Hydrate | 273 | 31.7 |
| 2 | Methane | 273 | 3.4 |
| 3 | Water saturated with methane | 298 | 31.7 |
| 4 | Hydrate | 150 | 0.1 |
| 5 | Hydrate | 150 | 10 |
| 6 | Hydrate | 150 | 100 |
| 7 | Hydrate | 150 | 400 |
| 8 | Hydrate | 250 | 10 |

The simulation box for methane hydrate consists of eight unit cells in a cubic arrangement of $2 \times 2 \times 2$. For the gaseous methane and the aqueous solution, the initial configuration was a simple cubic lattice. In all the simulations indicated in Table 2, 900,000 steps were used to equilibrate the system and the production phase lasted 400,000 additional steps. All parameters used in the simulations are specified in Table 3.

All the thermodynamic conditions for methane hydrates in Table 2 are included in the hydrate formation region according to the phase diagram reported in Sloan [1]. In all the analysed cases, the whole of the cavities was containing a methane molecule. Though the simulations do not measure the stability of the hydrates, because we are not making free energy calculations, the structure of the hydrates remains during the whole course of the simulation (Figure 2). This figure was generated by MOLDRAW [25] and presents a snapshot obtained from

Table 3. Parameters of the simulations.

| System | No. of molecules | No. of methane molecules | Time step, $\Delta t$ (fs) | Barostat relaxation time, $\tau_T$ (ps) | Thermostat relaxation time, $\tau_P$ (ps) |
|---|---|---|---|---|---|
| Methane hydrate | 432 | 64 | 0.8 | 0.0004 | 0.04 |
| Gaseous methane | 343 | 343 | 0.55 | 0.00005 | 0.0005 |
| Aqueous solution | 371 | 3 | 0.8 | 0.0004 | 0.04 |

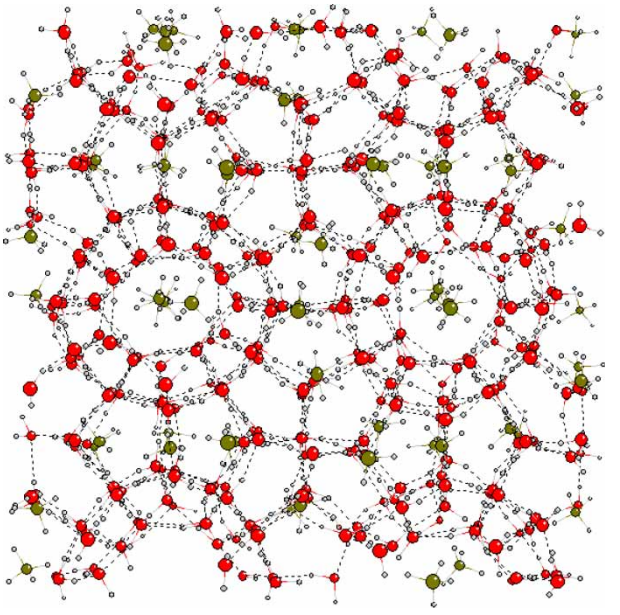

Figure 2. Snapshot of methane hydrate at 273 K and 31.7 MPa.

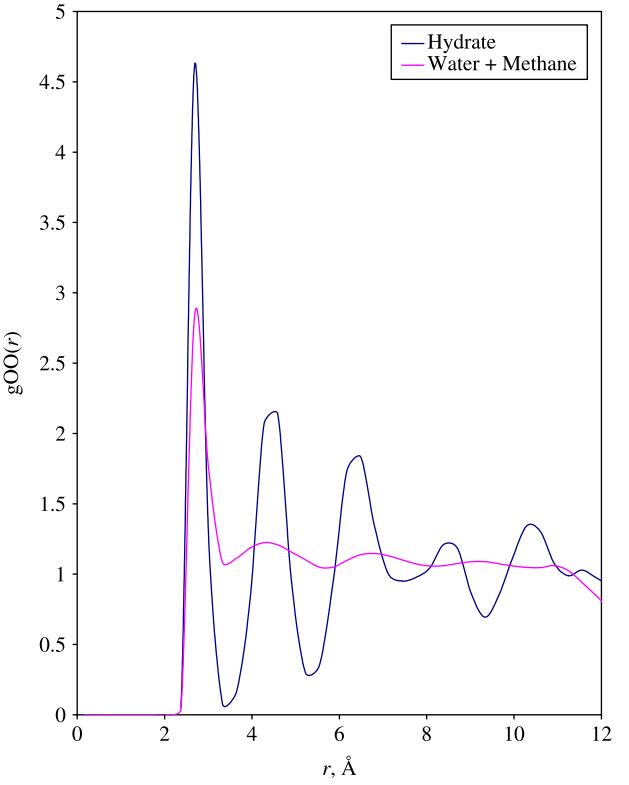


Figure 3. Radial distribution function for oxygen–oxygen in the water molecules of cases 1 and 3.

the simulation for conditions of 273 K and 31.7 MPa. In this figure, the large and small cages of the hydrate can be observed for the eight unit cells. The oxygen atoms are indicated in red, carbon in grey and hydrogen in white. The hydrogen bonds are represented by dashed lines, while the covalent bonds by continuous lines. The hydrate structure is preserved during the simulation as ratified by the radial distribution function (RDF). Figure 3 shows the RDF for oxygen–oxygen atoms of water molecules for cases 1 and 3. The RDF for case 1 presents the distinctive behaviour of a crystal, whereas the behaviour of a fluid phase is observed for case 3.

The equilibration of the system was monitored by the mean square displacement of a random molecule, and checking that this function increases when the disappearance of the initial structure for the gaseous methane and aqueous solution simulations has occurred. This parameter oscillates around a mean value for the methane hydrate simulations. In addition, the instantaneous values of the thermodynamic properties such as energy and density were monitored in all the simulations during the period of equilibration until these properties started to steadily oscillate about the mean values.

In the next sections, the behaviour with temperature, pressure and composition of each of the bands in the vibrational spectra for all the cases in Table 2 is discussed.

Table 4 indicates the frequency of the C—H symmetric stretch for cases 1–3, obtained by Raman spectroscopy and for the method of atomic velocity decomposition. The results obtained in the simulations for cases 1–3 agree with the tendencies observed for the experimental information. Figures 4 and 5 show the bands assigned to C—H symmetric and asymmetric stretching vibration, respectively, using the method of velocity decomposition. It is observed for both types of vibration in the hydrate that the assigned band divides into two peaks, one related to each type of cavity. The methane molecule in the large cavities has minor frequency than that in the small cavities, and, in turn, it has minor frequency with regard to the gaseous methane. The frequency for the C—H stretching vibrations in the small cavities is similar to the one present in the aqueous solution. Experimentally, the assignment of the bands in the Raman spectrum to the hydrate cages was based on peak intensities, but seems contradictory considering that methane in a large cavity has more translational freedom of motion, like methane gas, than methane in a small cage. In this work, the

Table 4. Vibrational frequencies of the C—H symmetric stretch.

| Case | Method | Frequency ($cm^{-1}$) |
|---|---|---|
| 1 | Experimental | 2915[a], 2905[b] |
| 1 | Simulation | 2878[a], 2870[b] |
| 2 | Experimental | 2917.3 |
| 2 | Simulation | 2940 |
| 3 | Experimental | 2911.3 |
| 3 | Simulation | 2874 |

[a] Small cage, [b] large cage.

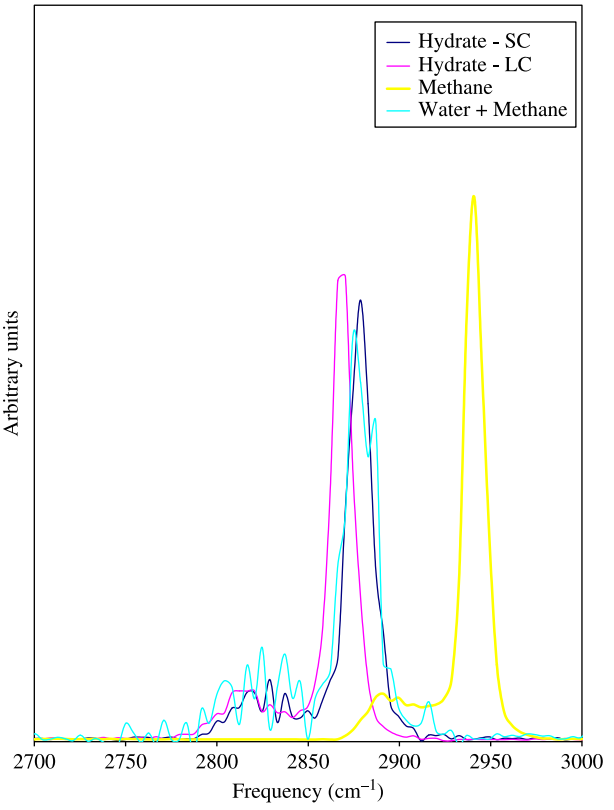


Figure 4. Vibrational spectrum of $Q_1$ for cases 1–3.

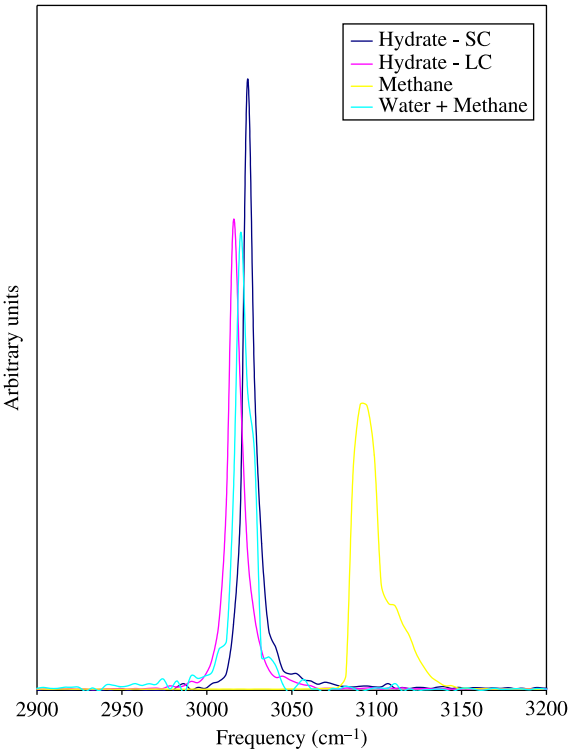


Figure 5. Vibrational spectrum of $Q_3$ for cases 1–3.

simulations permit a clear assignment of the bands to each cage in the hydrate. Although the frequencies calculated are not exactly experimental, the theoretically predicted trend of the C—H symmetric frequency (large cage < small cage ≈ water solution < gas) is in complete agreement with the experimental observation. The loose cage–tight cage model [26] explains the shift observed in C—H stretching frequencies for methane trapped in the hydrate; in the large cage, methane has a looser cage environment and, therefore, a minor frequency of the stretching vibration with regard to the small cage.

Figure 6 shows the spectrum obtained through the Fourier transform of the VACF for the carbon atom. It is observed that, with this method, a differentiation is obtained in the frequencies of vibration for the large and small cages in spite of the oscillations, and that the frequencies in the large cage happen to be minor frequencies. The simulation of the gaseous methane produces a single band in the region of 0–500 cm$^{-1}$, where the motions at low frequency (librations) occur. In the case of the aqueous solution, due to such a small quantity of methane molecules, a major number of oscillations are produced impeding to be able to distinguish some band in specific. The disadvantage of this method is that it is not possible to assign any one of the bands observed to a specific vibration, as in the case of the method of velocity decomposition.

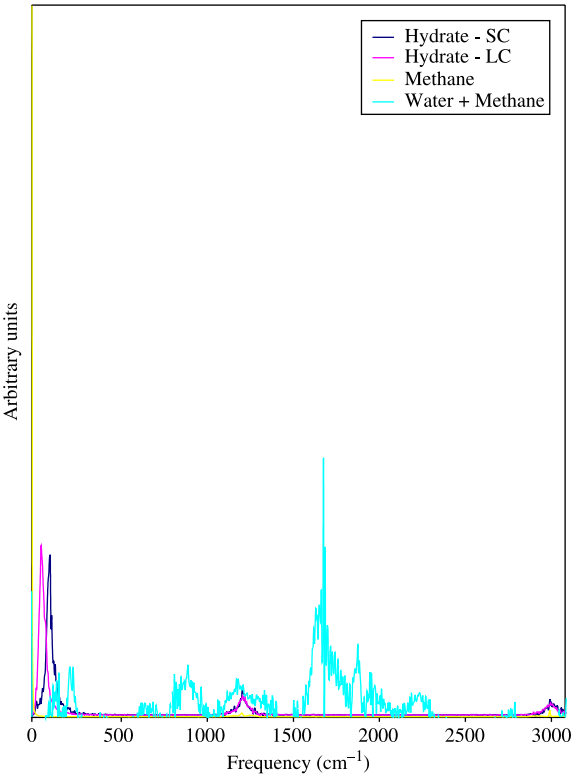


Figure 6. Vibrational spectrum obtained from the carbon velocities for cases 1–3.

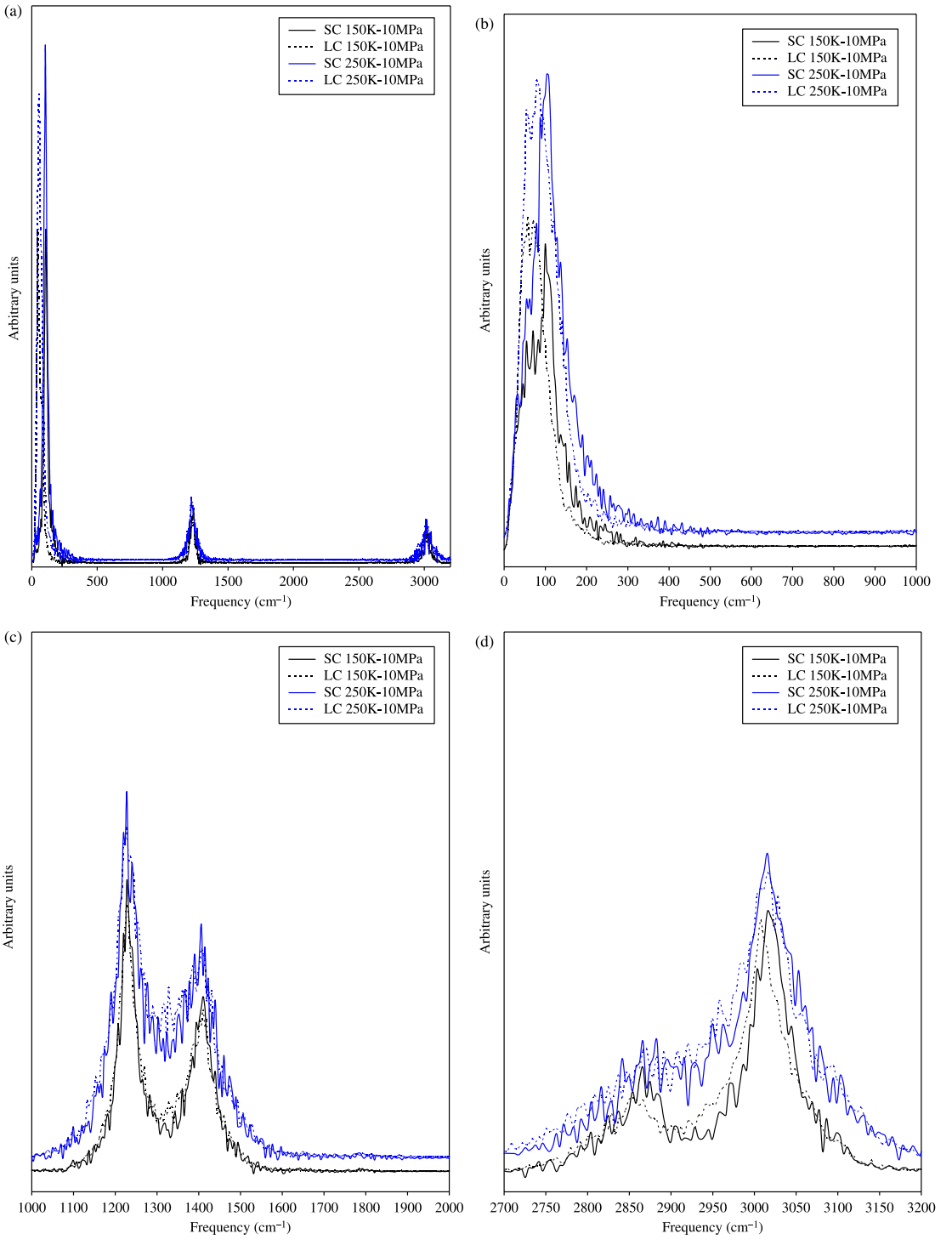


Figure 7. Temperature effect in the vibrational spectrum obtained from (a) carbon and (b–d) hydrogen velocities.

### *3.1 Temperature effect*

The cases 5 and 8 shown in Table 2 were analysed to observe the effect of the temperature in the vibrational spectra of carbon and hydrogen with the Fourier transform of the VACF (Figure 7(a)–(d)). There are two bands in the region, between 0 and 500 $cm^{-1}$, observed in the carbon spectrum, which correspond to the librational motions of methane molecules in the large and small cavities. The band of $\sim 1240\,cm^{-1}$ corresponds to the bending vibrations, while the band of $\sim 3000\,cm^{-1}$ corresponds to the C—H stretch.

The vibrational spectrum of hydrogen was divided into several parts for the sake of clarity. The two bands in

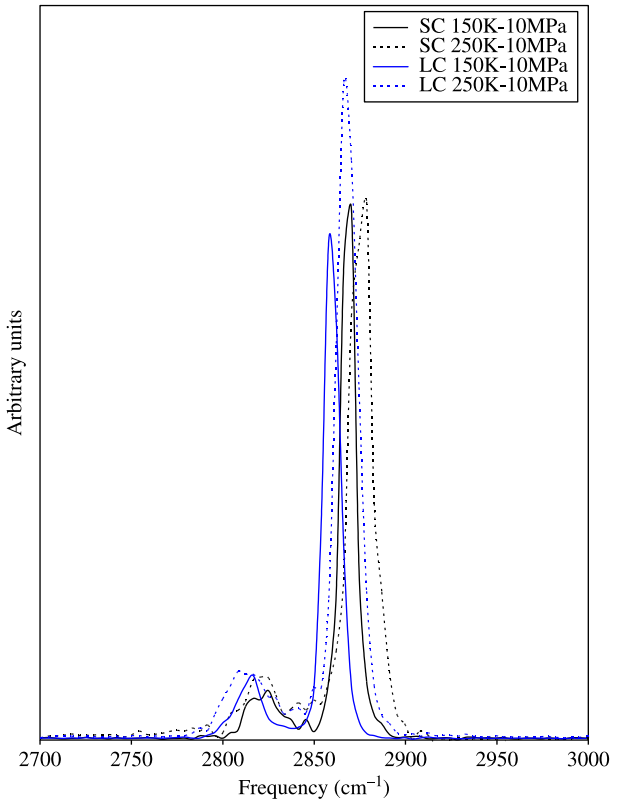


Figure 8. Vibrational spectrum of $Q_1$ for cases 5 and 8.

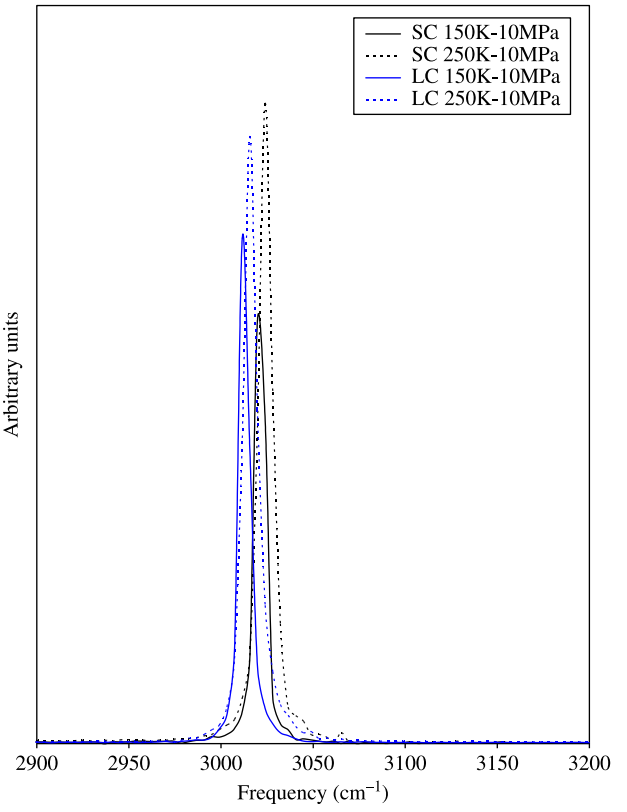


Figure 9. Vibrational spectrum of $Q_3$ for cases 5 and 8.

the region between 1000 and 1500 cm$^{-1}$ correspond to the bending modes in the methane molecule. Greathouse and Cygan [15] report the frequency of these bands (1304 and 1520 cm$^{-1}$) for MD simulations of methane hydrate at 273 K, while Jiang et al. [16] report them (1352 and 1511 cm$^{-1}$) at 200 K and 20 bar, respectively. In the present study, the bands corresponding to the symmetric and asymmetric C—H stretching are those appearing in the 2800–3100 cm$^{-1}$ region. Greathouse and Cygan [15] report the frequency of these bands as 2826 and 2842 cm$^{-1}$ for symmetric stretching in the large and small cages, respectively, and as 2986 and 3000 cm$^{-1}$ for asymmetric vibration in the large and small cages, respectively. The spectrum in Figure 7(d) shows similar information for the symmetric and asymmetric C—H stretch. It is also possible to observe a small difference in the frequencies for the asymmetric C—H stretching between the small and large cages. In the present study, a raise in temperature increases the band's frequency for the librational motions and C—H stretching vibrations, their effect being almost imperceptible on the bending and rocking modes. The spectrum calculated from the VACF includes not only the stretching vibrations but also other types of motions such as bending, libration and translation. Hence, there is no clear difference between the cages for the frequency of the C—H symmetric stretching.

In Figures 8 and 9, the frequencies of symmetric, $Q_1(t)$, and asymmetric, $Q_3(t)$, stretching are shown for methane in the small and large cavities at different temperatures using the proposed procedure. When using this method in each of the spectra, it only appears as the band related to the vibrational mode. The C—H symmetric stretching is one of the vibrational modes with more importance in the spectroscopic analysis of methane hydrates. Sum et al. [5] report a difference in the frequency for this mode between the large and small cavities of 10 cm$^{-1}$. The difference between the large and small cavities is $\sim$12 cm$^{-1}$ for both temperatures (Figure 8); however, the bands of the C—H symmetric stretching appear with smaller frequencies at lower temperatures. Also, there is an increment in the frequency of the bands for the C—H asymmetric stretching due to the increase in the temperature (Figure 9). The band of the C—H asymmetric stretching appears with a difference of $\sim$8 cm$^{-1}$ between the large and small cavities for both temperatures. The principal advantage of this method is that the bands that appear in the spectrum relate directly to the analysed vibration and especially when they appear with major definition than in the spectrum obtained by the traditional method.

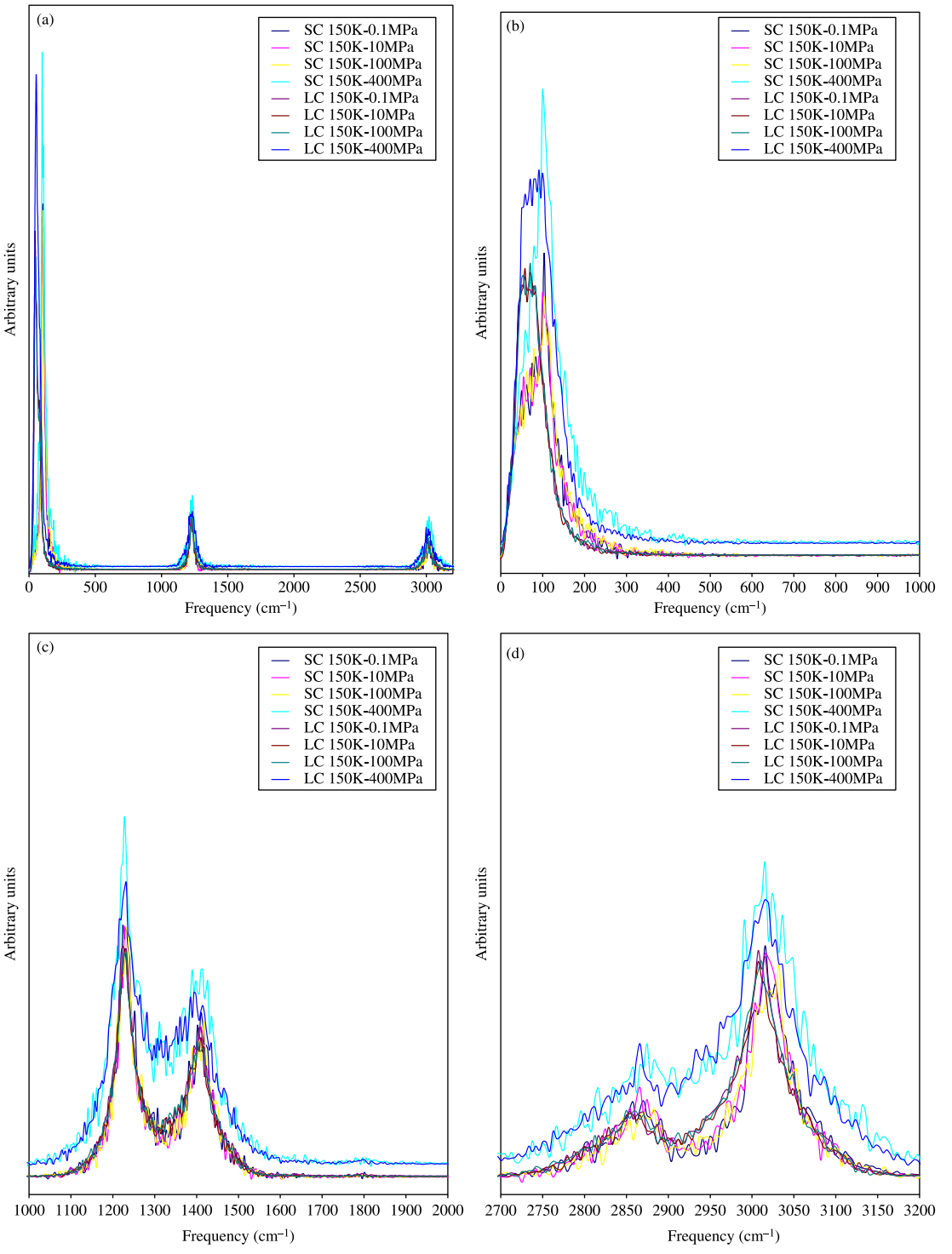


Figure 10. Pressure effect in the vibrational spectrum obtained from (a) carbon and (b–d) hydrogen velocities.

### *3.2 Pressure effect*

Cases 4–7 from Table 2 were used here to observe the changes of pressure in the vibrational spectrum. Figure 10(a)–(d) shows the results obtained from the atomic velocity method for the carbon and hydrogen in the methane molecule. In the region where the librational motions ($0-500\,cm^{-1}$) are obtained, differences were observed in the frequencies for the small and large cavities in the carbon spectrum. In this same spectrum, the other two bands that correspond to the bending and stretching

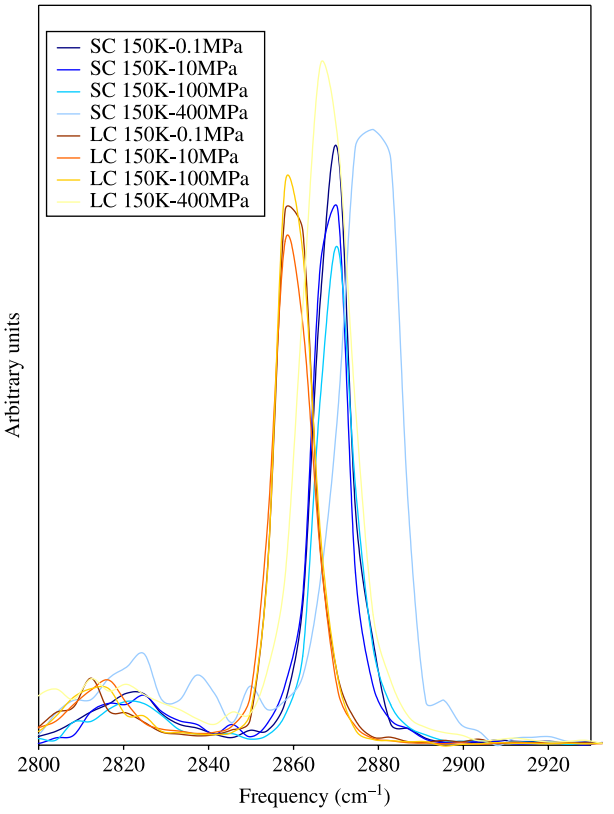


Figure 11. Vibrational spectrum of $Q_1$ for cases 4–7.

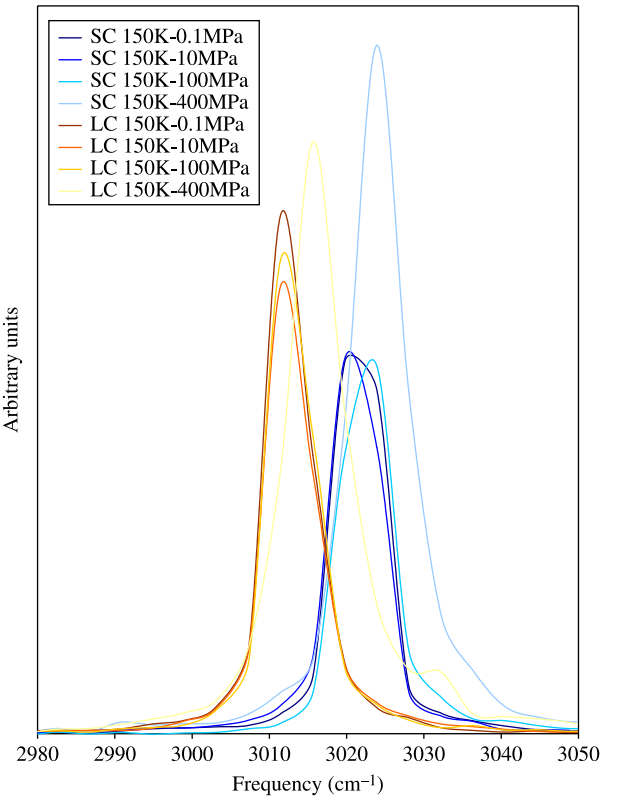


Figure 12. Vibrational spectrum of $Q_3$ for cases 4–7.

modes are observed. The bands for the bending and stretching modes are observed in more detail in the hydrogen spectrum. No meaningful difference is detected in this method for the carbon or hydrogen spectra in the frequencies and form of the bands by the effect of pressure changes.

Figures 11 and 12 show the spectra obtained with the method of velocity decomposition for cases 4–7 from Table 2. It is observed that changes in pressure have a considerable effect in the frequencies of the C—H stretching. The change in pressure analysed in this work for cases 4–6 is not probably sufficiently big to clearly produce a change in the frequencies of vibration modes of the hydrate. However, for case 7, a significant pressure effect occurs for both types of cages. The difference in the frequencies between the large and small cages is approximately 12 cm$^{-1}$ for symmetric and 8 cm$^{-1}$ for asymmetric stretching.

Nakano et al. [24] have reported that the frequency of the C—H symmetric stretching vibration of methane in small cages of sI hydrate increases monotonically with pressure and the frequency for methane in the large cages remains almost constant over the range of 0–500 MPa. In this work, we predicted the same behaviour for the increment in frequency for small cages; however, we also report an increment in the frequency for large cages.

## 4. Conclusions

The thermodynamic conditions of each simulation in this work affect in a significant way the vibrational spectra. Though polarisable potentials have been used for hydrate molecules in other works [15,16] thinking in the best reality emulation, the main disadvantage in comparison to using effective potentials is that they require greater execution time. Nevertheless, the results obtained in this work, which uses effective potentials, requiring less computational effort, are comparable to the results obtained in previous studies, and there was also good agreement between predicted and observed trends for the C—H stretching frequencies. In each one of the results, differences in the frequency between the large and small cages were observed to be of approximately 12 cm$^{-1}$ and the bands of the large cavities always appear at smaller frequencies than those corresponding to the small cavities. This result satisfactorily agrees with that reported by Sum et al. [5].

In this work, a better definition of vibrational spectra is achieved with the method of velocity decomposition. This method allows the decomposition and assignation of the bands which appear in the spectrum at specific vibrations when choosing a spectroscopic property associated with that motion. The results obtained indicate that the temperature rebounds in a remarkable way in the vibrational spectrum, increasing the frequencies of

the bands for translational and stretching motions when the temperature increases. These changes in temperature did not significantly affect the spectrum of the bending and rocking modes. The increase in pressure also produces changes in the vibrational spectrum. The most noticeable change with increasing pressure was observed in the spectrum obtained from the method of velocity decomposition for the C—H symmetric and asymmetric vibrations. The C—H stretching in both cages of methane hydrates increases with pressure possibly due to a decrease in the space for the methane molecules in the cages by pressurisation.

MD simulations have been used in this work to understand the dynamic behaviour of methane hydrates and to explain some of the experimental findings in the vibrational spectra for these systems. This kind of information can be useful when there is a need to develop experimental studies at high temperatures and pressures, where performing these experiments becomes difficult and highly unsafe.



## References


[1] E.D. Sloan, *Clathrate Hydrates of Natural Gases*, Marcel Dekker, New York, 1998.

[2] H. Hirai, T. Kondo, M. Hasegawa, T. Yagi, Y. Yamamoto, T. Komai, K. Nagashima, M. Sakashita, H. Fujihisa, and K. Aoki, *Methane hydrate behaviour under high pressure*, J. Phys. Chem. B 104 (2000), pp. 1429–1433.

[3] K.A. Udachin, C.I. Ratcliffe, and J.A. Ripmeester, *Single crystal diffraction studies of structure I, II and H hydrates: Structure, cage occupancy and composition*, J. Supramol. Chem. 2 (2002), pp. 405–408.

[4] J.A. Ripmeester and C.I. Ratcliffe, *Low-temperature cross-polarization/magic angle spinning 13C NMR of solid methane hydrates: Structure, cage occupancy, and hydration number*, J. Phys. Chem. 92 (1988), pp. 337–339.

[5] A.K. Sum, R.C. Burrus, and E.D. Sloan, *Measurement of clathrate hydrates via Raman spectroscopy*, J. Phys. Chem. B 101 (1997), pp. 7371–7377.

[6] E.D. Sloan, S. Subramanian, P.N. Matthews, J.P. Lederhos, and A.A. Khokar, *Quantifying hydrate formation and kinetic inhibition*, Ind. Eng. Chem. Res. 37 (1998), pp. 3124–3132.

[7] S. Subramanian and E.D. Sloan, *Molecular measurements of methane hydrate formation*, Fluid Phase Equ. 158 (1999), pp. 813–820.

[8] H. Shimizu, T. Kumazaki, T. Kume, and S. Sasaki, In situ *observations of high pressure phase transformations in a synthetic methane hydrate*, J. Phys. Chem. B 106 (2002), pp. 30–33.

[9] J.H. Yoon, T. Kawamura, Y. Yamamoto, and T. Komai, *Transformation of methane hydrate to carbon dioxide hydrate:* In situ *Raman spectroscopic observations*, J. Phys. Chem. A 108 (2004), pp. 5057–5059.

[10] J.S. Tse, C.I. Ratcliffe, B.M. Powell, V.F. Sears, and Y.P. Handa, *Rotational and traslational motions of trapped methane. Incoherent inelastic neutron scattering of methane hydrate*, J. Phys. Chem. A 101 (1997), pp. 4491–4495.

[11] J.S. Tse, M.L. Klein, and I.R. McDonald, *Molecular dynamics studies of ice Ic and the structure I clathrate hydrate of methane*, J. Phys. Chem. 87 (1983), pp. 4198–4203.

[12] J.S. Tse, M.L. Klein, and I.R. McDonald, *Computer simulation studies of the structure I clathrate hydrates of methane, tetrafluoromethane, cyclopropane, and ethylene oxide*, J. Chem. Phys. 81 (1984), pp. 6146–6153.

[13] H. Itoh and K. Kawamura, *Molecular dynamics simulations of clathrate hydrate. Intramolecular vibrations of methane*, Ann. New York Acad. Sci. 912 (2000), pp. 693–701.

[14] N.J. English and J.M.D. MacElroy, *Structural and dynamical properties of methane clathrate hydrates*, J. Comput. Chem. 24 (2003), pp. 1569–1581.

[15] J.A. Greathouse and R.T. Cygan, *Vibrational spectra of methane clathrate hydrates from molecular dynamics simulation*, J. Phys. Chem. B 110 (2006), pp. 6428–6431.

[16] H. Jiang, K.D. Jordan, and C.E. Taylor, *Molecular dynamics simulations of methane hydrate using polarizable force fields*, J. Phys. Chem. B 111 (2007), pp. 6486–6492.

[17] J. Martí, J.A. Padró, and E. Guardia, *Computer simulation of molecular motions in liquids: Infrared spectra of water and heavy water*, Mol. Simul. 11 (1993), pp. 321–336.

[18] O. Teleman, B. Jönsson, and S. Engström, *A molecular dynamics simulation of a water model with intramolecular degrees of freedom*, Mol. Phys. 60 (1987), pp. 193–203.

[19] W.L. Jorgensen, D.S. Maxwell, and J. Tirado-Rives, *Development and testing of the OPLS all-atom force field on conformational energetics and properties of organic liquid*, J. Am. Chem. Soc. 118 (1996), pp. 11225–11236.

[20] W.C. Swope, H.C. Andersen, P.H. Berens, and K.R. Wilson, *A computer simulation method for the calculation of equilibrium constants for the formation of physical clusters of molecules: Application to small water clusters*, J. Chem. Phys. 76 (1982), pp. 637–649.

[21] H.J.C. Berendsen, J.P.M. Postma, W.F. van Gunsteren, A. di Nola, and J.R. Haak, *Molecular dynamics with coupling to an external bath*, J. Chem. Phys. 81 (1984), pp. 3684–3690.

[22] P. Bopp, *A study of the vibrational motions of water in an aqueous $CaCl_2$ solution*, Chem. Phys. 106 (1986), pp. 205–212.

[23] H. Wu, S. Sasaki, and H. Shimizu, *High-pressure Raman study of dense methane*, J. Raman Spectrosc. 26 (1995), pp. 963–967.

[24] S. Nakano, M. Moritoki, and K. Ohgaki, *High-pressure phase equilibrium and Raman microprobe spectroscopic studies on the methane hydrate system*, J. Chem. Eng. Data 44 (1999), pp. 254–257.

[25] P. Ugliengo, D. Viterbo, and G. Chiari, *MOLDRAW: Molecular graphics on a personal computer*, Z. Kristallogr. 207 (1993), pp. 9–23.

[26] G.C. Pimentel and S.W. Charles, *Infrared spectral perturbations in matrix experiments*, Pure Appl. Chem. 7 (1963), pp. 111–123.